Experimental and Theoretical Studies of the Colloidal Stability of Nanoparticles—A General Interpretation Based on Stability Maps

Doris Segets,[§,†] Renata Marczak,[§,†] Stefan Schäfer,[§,†] Carolin Paula,[†] Jan-Frederik Gnichwitz,[‡] Andreas Hirsch,[‡] and Wolfgang Peukert[†,*]

[†]Institute of Particle Technology, Friedrich-Alexander-University Erlangen-Nuremberg, Cauerstrasse 4, 91058 Erlangen, Germany and [‡]Department of Chemistry and Pharmacy & Interdisciplinary Center of Molecular Materials (ICMM), Friedrich-Alexander-University Erlangen-Nuremberg, Henkestrasse 42, 91054 Erlangen, Germany. [§]These authors contributed equally to this work.

ABSTRACT The current work addresses the understanding of the stabilization of nanoparticles in suspension. Specifically, we study ZnO in ethanol for which the influence of particle size and reactant ratio as well as surface coverage on colloidal stability in dependence of the purification progress was investigated. The results revealed that the well-known ζ-potential determines not only the colloidal stability but also the surface coverage of acetate groups bound to the particle surface. The acetate groups act as molecular spacers between the nanoparticles and prevent agglomeration. Next to DLVO calculations based on the theory of Derjaguin, Landau, Verwey and Overbeek using a core—shell model we find that the stability is better understood in terms of dimensionless numbers which represent attractive forces as well as electrostatic repulsion, steric effects, transport properties, and particle concentration. Evaluating the colloidal stability in dependence of time by means of UV—vis absorption measurements a stability map for ZnO is derived. From this map it becomes clear that the dimensionless steric contribution to colloidal stability scales with a stability parameter including dimensionless repulsion and attraction as well as particle concentration and diffusivity of the particles according to a power law with an exponent of −0.5. Finally, we show that our approach is valid for other stabilizing molecules like cationic dendrons and is generally applicable for a wide range of other material systems within the limitations of vanishing van der Waals forces in refractive index matched situations, vanishing ζ-potential and systems without a stabilizing shell around the particle surface.

KEYWORDS: ZnO · nanoparticles · quantum dots · stability · core—shell model · DLVO theory · stability map · dimensional analysis

ZnO semiconductor quantum dots have attracted considerable attention owing to their promising electro-optical properties. Besides fundamental research on the particle synthesis itself,[1−4] especially the application of nanoparticles for electronic devices[5] or solar cells[6−8] is increasingly in the focus of interest. However, for the successful incorporation of nanoparticles into devices, stable suspensions at high solid concentrations are required. At first glance, the stabilization of small nanoparticles seems to be rather challenging as the collision events between the particles are supposed to be very frequent due to the strong influence of Brownian motion in the lower nanometer range. In contrast, experiments have revealed that ZnO and other nanoparticles below 10 nm in diameter made of other materials, like noble metals from gold, silver, or other quantum dot systems like cadmium sulfide or titanium dioxide, can be stored over months at room temperature without noticeable aggregation.[9,10]

Colloidal stability is usually discussed in terms of electrostatic repulsion, steric stabilization, and electrosteric stabilization as a combination of the former ones.[11] Regarding electrostatic stabilization, an electric double layer around the nanoparticle surface is created. As identical particles have the same sign of their surface charge they reject each other when they approach. In the case of steric stabilization, molecules adsorbed or bound to the particle surface create a protecting layer around the nanoparticles. This layer can be seen as spacer and prevents particles from coming close enough to agglomerate due to attractive van der Waals forces which become stronger with decreasing particle—particle distance. Finally, electrosteric stabilization is achieved by means of charged molecules including polyelectrolytes and represents a combination of the aforementioned stabilization techniques.

Usually, the well-known Derjaguin—Landau—Verwey—Overbeek (DLVO) theory[12,13] is used to calculate total interaction potentials around a particle surface assuming a superposition between repulsive forces, for example, electrostatic repulsion, Born

* Address correspondence to W.Peukert@lfg.uni-erlangen.de.

Received for review February 4, 2011 and accepted April 27, 2011.

Published online May 05, 2011
10.1021/nn200465b

repulsion, and attractive forces like van der Waals attraction. Thereby, a typical DLVO-curve shows a primary maximum which has to be maximized to achieve good colloidal stability.[14] However, with the application of this concept toward small particles below 20 nm the corresponding absolute interaction potentials with only a few kT become rather small.[15,16] Thus, if aggregation has already been induced—like the destabilization of gold nanoparticles due to the replacement of citrate ions at the particle surface by benzyl mercaptane[17,18] or the destabilization of CdSe quantum dots due to the addition of an electrolyte[19]—the observed phenomena are explained on the basis of classical DLVO theory, although only slight changes occur in the height and position of the repulsive maximum. In contrast, the *a priori* prediction of the stability of a suspension with small nanoparticles is challenging, and thus a lot of experiments are required. Recently, we have shown that there exists an optimum of colloidal stability during the washing of ~5 nm ZnO quantum dots in ethanolic suspension.[16] This was explained using an extended core–shell model of the well-known DLVO theory which considers not only the surface charge of the nanoparticles but also a protecting shell of acetate ions around them.[16,20–22] The conclusion was that during washing these acetate ions are removed from the particle surface until the "steric" stabilization breaks down and flocculation is observed.

However, the total interaction potential did only change slightly for each washing step. The well-known stability criterion, that the repulsive maximum should be larger than 15 kT, was clearly not fulfilled, although the quantum dot suspensions were stable over months. In the current work a dimensional analysis was applied for the case of charged nanoparticles surrounded by stabilizing ions or molecules in a solvent to find generally applicable conditions for colloidal stability. By means of dimensional analysis[23] a set of nine independent dimensionless Π-products was identified, which includes next to particle volume fraction and dimensionless diffusion also dimensionless parameters for repulsion and attraction, respectively, and a geometry factor taking into account the thickness of the protecting shell around the particle surface. Thus, a stability map could be constructed which enables a clear predictive statement if the ZnO quantum dots are stable within a certain time for different particle sizes, ζ-potentials, synthesis conditions, and washing steps. Furthermore, our stability map was extended toward various other material systems with different adsorbed ions or molecules sitting at the particle surface.

RESULTS AND DISCUSSION

Measurement Data: ζ-Potential, pH*, and Surface Coverage. Crystalline ZnO quantum dots were formed after mixing ethanolic solutions of the precursors, that is, zinc acetate dihydrate and lithium hydroxide, at 20 °C and 35 °C, respectively, under vigorous stirring. Three different reactant ratios $[Zn^{2+}]/[OH^-]$ of 1/1, 1/1.5, and 1/2 were used during the synthesis. To follow the progress of oxide formation, the suspensions of the nanoparticles were aged in their mother liquors and the crystal growth was monitored by UV–vis absorption spectroscopy. Furthermore, particle size distributions (PSDs) at different aging time were constructed from the conversion of the absorption spectra using an algorithm already published in the literature.[1] However, as the main goal of the current work is the investigation of colloidal stability of ZnO quantum dots in ethanolic suspension, a detailed analysis of the particle growth with respect to the reactant ratios $[Zn^{2+}]/[OH^-]$ is shown in the Supporting Information for both temperatures (S1). For a more detailed examination of the colloidal stability and the surface charge of the nanoparticles, the ζ-potential, the surface coverage of acetate ions relative to a monolayer as well as the pH* were determined for both temperatures (Figure 1 and Table 1, respectively). In principle all results were similar; therefore, herein we only show the data for 20 °C. The corresponding results at 35 °C are presented in the Supporting Information (S2). The ζ-potential, the surface coverage, and the pH* were measured for the reactant ratios $[Zn^{2+}]/[OH^-]$ of 1/1 and 1/1.5 in the unwashed suspensions after synthesis as well as after the first, the second, and the third washing cycle. However, regarding the samples with $[Zn^{2+}]/[OH^-]$ of 1/2, pH* and ζ-potential could only be determined for the unwashed suspension and the suspension after the first washing cycle due to the fact that the particles became unstable and could not be redispersed after the second precipitation with heptane.

Regarding the suspension with a reactant ratio $[Zn^{2+}]/[OH^-]$ of 1/1 (Figure 1a, red squares), the magnitude of the negative ζ-potential increases with the first washing step by more than 10 mV from −14 mV to −28 mV. This is ascribed to the removal of dissolved ions from the suspension leading to a decrease of the ionic strength. Then, the ionic strength reduction leads to an increased thickness of the electric double layer around the nanoparticles.

However, ongoing washing leads to a decrease of the absolute value of the ζ-potential down to −22 mV after the second purification step and a final value of −4.8 mV after the third washing cycle. To understand this behavior the removal of acetate ions coordinated with the particle surface has to be considered (see results of the thermo gravimetric analysis (TGA) measurements with respect to the washing progress shown in Figure 1b) as these specifically adsorbed ions cause the negative surface charge of the particles after synthesis. Thereby acetates are associated with the particle surface according to the well-known bonding structures for acetate groups

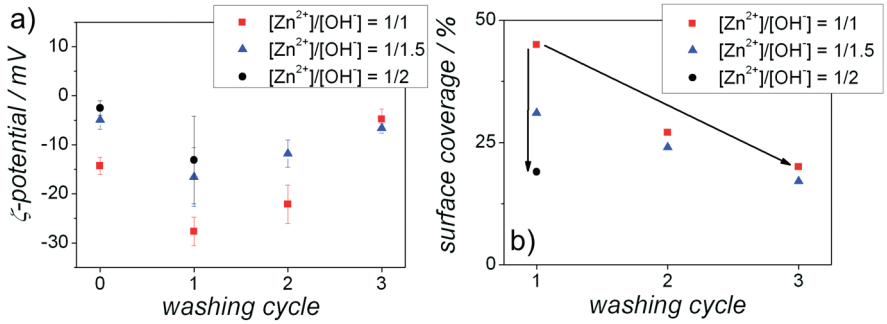

Figure 1. (a) ζ-potentials for the different reactant ratios $[Zn^{2+}]/[OH^-]$ of 1/1 (red squares), 1/1.5 (blue triangles), and 1/2 (black circles) after zero, one, two, and three washing cycles (ZnO quantum dots with size of about 2 nm) at 20 °C; (b) corresponding percentage surface coverage of the particles with acetate ions in dependence of the washing cycles at 20 °C; the data points for the suspensions synthesized in a reactant ratio $[Zn^{2+}]/[OH^-]$ of 1/2 are not included because the particles were strongly agglomerated after more than one cycle of washing.

TABLE 1. Effective Acetate Shell Thickness *d* (eq 1) and pH* Values (Provided That the Particles Were Sufficiently Stable to Perform a pH* Measurement) for the Three Different Reactant Ratios $[Zn^{2+}]/[OH^-]$ of 1/1, 1/1.5, and 1/2 after Zero, One, Two, and Three Washing Cycles (ZnO Quantum Dots with Size of about 2 nm)

	acetate shell thickness *d* (nm)			pH*		
	$[Zn^{2+}]/[OH^-]$ = 1/1	$[Zn^{2+}]/[OH^-]$ = 1/1.5	$[Zn^{2+}]/[OH^-]$ = 1/2	$[Zn^{2+}]/[OH^-]$ = 1/1	$[Zn^{2+}]/[OH^-]$ = 1/1.5	$[Zn^{2+}]/[OH^-]$ = 1/2
unwashed	0.470	0.470	0.470	6.7 ± 0.7	7.1 ± 0.7	7.9 ± 0.7
1× washed	0.212	0.146	0.089	7.0 ± 0.7	7.1 ± 0.7	8.2 ± 0.7
2× washed	0.127	0.113		6.9 ± 0.7	7.1 ± 0.7	
3× washed	0.094	0.080		7.0 ± 0.7		

coordinated with a metal, namely unidentate, bidentate (chelate), or bridging mode. This was reported in detail by Sakohara *et al.*[24] and confirmed by the recently published work of Marczak *et al.*[25] Sakohara *et al.* found that the type of bonding is directly influenced by the reactant ratio and that colloidal stability depends on the amount of acetate at the particle surface.

Furthermore, from the weight loss during TGA, the thicknesses of the acetate shells with respect to the washing cycle were calculated and are presented in Table 1. The percentage fraction of a monolayer is calculated from the weight loss and the known particle diameter from UV–vis absorption spectroscopy as already described in the literature.[16] Then, the effective shell thickness is calculated assuming no cross-linking hydroxide being present at the particle surface according to

$$d = \frac{A}{100} d_{\text{max, monolayer}} \quad (1)$$

where d is the effective thickness of the acetate shell, A is the surface coverage in percent, and $d_{\text{max, monolayer}}$ is the theoretical maximum shell thickness of a monolayer of acetate molecules at the particle surface. The latter was estimated (MM2 force field calculation method, Chem Pro 3D 11.0, CambridgeSoft, UK) to be 0.47 nm. Figure 1b and Table 1 demonstrate that with the second and third washing the charge determining coordinating ions are removed from the particle surface and the surface without acetate ions must be taken into account. This "naked" surface is now supposed to be positive because the measured pH* is situated below the isoelectric point of ZnO at pH^*_{iep} 9.[26] This was recently reported by Tang *et al.*,[27] who synthesized ZnO from anhydrous zinc acetate and measured the pH* dependence of the ζ-potential between pH* 6 and pH* 12. Thus, the ζ-pH* dependence of ZnO in ethanol is, in a first instance, comparable to the already reported results for aqueous ζ-pH measurements.[28] However, a generic problem exists in situations where the ζ-potential is poorly defined, *i.e.*, in most nonaqueous solutions in which, nevertheless, charge stabilization may be effective. In these cases the ζ-potential should be replaced by the surface potential which may be obtained by charge titration experiments.

The suspension with the $[Zn^{2+}]/[OH^-]$ of 1/1.5 (Figure 1a and b, blue triangles) follows the same trend, that is an increase of the magnitude of the ζ-potential after the first washing due to a reduction of the ionic strength of the suspension and a subsequent decrease of the magnitude of the ζ-potential with the second and third washing. Thereby, except after the third washing cycle, the magnitude of the ζ-potential is always lower in comparison to the sample with an equimolar reactant ratio. This is again in good agreement with the evolution of the surface coverage.

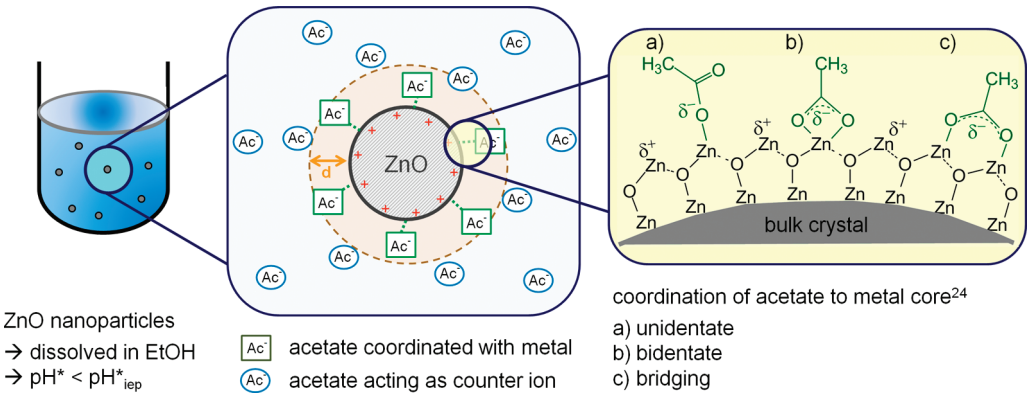

Scheme 1. Schematic drawing of the chemical surrounding of the ZnO quantum dots stabilized with acetates that are either coordinated to the particle surface[24] or acting as counterion.

In general, the surface coverage of acetate ions decreases with increasing amount of LiOH leading to smaller ζ-potentials. However, for the three times washed samples the trend is slightly opposite. In this case the magnitude of the ζ-potential for the 1/1 reactant ratio is smaller than the ζ-potential for the $[Zn^{2+}]/[OH^-]$ of 1/1.5. This is explained by considering the intrinsic charge of the ZnO nanoparticles for the three times washed samples. The pH* at a ratio of 1/1.5 is always higher than the pH* at $[Zn^{2+}]/[OH^-]$ of 1/1. Thus, according to the literature the corresponding intrinsic surface charge becomes smaller with increasing hydroxide concentration as the sample synthesized for $[Zn^{2+}]/[OH^-]$ of 1/1.5 is closer to the pH^*_{iep} than the sample synthesized for 1/1.[27]

For the suspension synthesized for a reactant ratio of 1/2 this trend is expected to continue as the pH* increases further up to pH* 8 after the first washing. However, determination of the corresponding values was not possible due to the strong instability of those samples. Finally, the following findings have been derived: (i) The acetate surface coverage of the nanoparticles decreases both with each washing step and with increasing excess of hydroxide ions. (ii) The magnitude of the ζ-potential increases with the first washing for all investigated reactant ratios but decreases with the second and third washing step. Thereby it approaches a pH*-dependent surface charge as during washing the charge determining acetate ions are continuously removed and only a small amount of coordinated acetate remains at the particle surface. To illustrate this further, Scheme 1 shows a drawing of the chemical surrounding of the ZnO quantum dots consisting of an intrinsic positive surface charge, a small amount of either acetate ions acting as counterions, or acetate ions being coordinated to the particle surface. The detailed chemistry of acetates coordinated to the ZnO nanoparticle surface according to Sakohara *et al.* is presented in the enlargement.[24]

Core–Shell Model of DLVO Theory. The interaction potentials at the minimal contact distance between the ZnO quantum dots after the different washing steps were calculated for a temperature of 20 °C according to the DLVO theory[12,13] based on a core–shell model and are shown in Figure 2a.[15,16,29,30] Correspondingly, also the stability ratios *W* were calculated as the sum of the electrostatic repulsion, the van der Waals forces, and the Born repulsion according to Lagaly *et al.*[14] which are shown in Figure 2b. The Born repulsion was approximated by a hard sphere potential at the minimal contact distance of 0.16 nm.[31] Moreover, a stabilizing acetate shell around the particle surface was considered in the calculations. All the details about the parameters used for the calculations and the corresponding data for a synthesis temperature of 35 °C are described in the Supporting Information (S3 and S5, respectively).

According to the literature, a suspension is typically considered to be stable if the total interaction potential reveals an energy barrier larger than 15 kT and stability factors of $W > 10^5$.[31] Obviously, this criterion is insufficient to explain stability for particle sizes that are significantly smaller than 20 nm. The calculations for the ZnO quantum dot system have shown that the maximum repulsion is only in the order of 1 kT. However, the attractive van der Waals term is also rather small due to the small particle size. Thus, a subnanometer shell effectively screens the attractive force so that essentially a hard-core-potential.[15,16] Comparative calculations for other quantum dot systems show a similar trend. Therefore, the stability criteria have to be extended especially for quantum dots. It was recently shown that not only the height of the energy barrier but also the depth of the primary minimum of the total interaction potential should be considered.[15,16] Despite that the values are small within the experimental error that mainly comes from the determination of the ζ-potential, still a weak trend in the depth of the primary minimum as well as the stability ratio during washing is observed as already described in our previous work.[16] Therefore, a proper application of DLVO-theory reflects the stability of quantum dots in agreement with the experimental findings. However, the DLVO approach is not

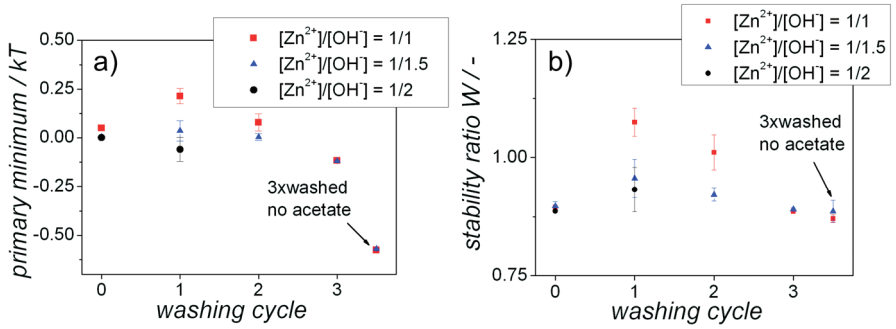

Figure 2. (a) Primary minima at the minimal contact distance of 0.16 nm at 20 °C and (b) stability ratios *W* calculated according to core–shell model of DLVO theory for 2 nm ZnO quantum dots synthesized with reaction ratios $[Zn^{2+}]/[OH^-]$ of 1/1 (red squares), 1/1.5 (blue triangles), and 1/2 (black circles) at 20 °C. Additionally, the values for a complete removal of the acetate shell ($d = 0$) are shown and indicated with an arrow.

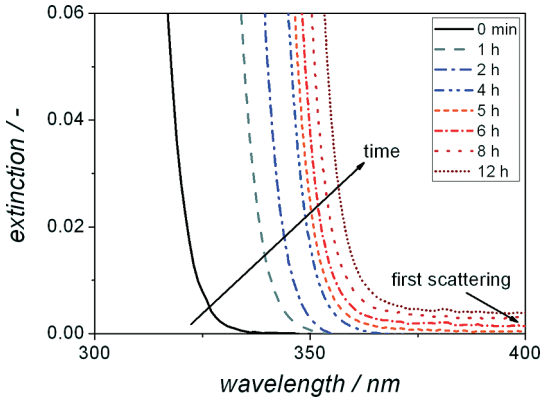

Figure 3. UV–vis absorption spectra recorded at different aging times of unwashed ZnO quantum dots synthesized with reactant ratio $[Zn^{2+}]/[OH^-]$ of 1/2 and a temperature of 20 °C; the small maximum of the measurement data around $\lambda = 380$ nm comes from the switch between the visible and the UV lamp, respectively.

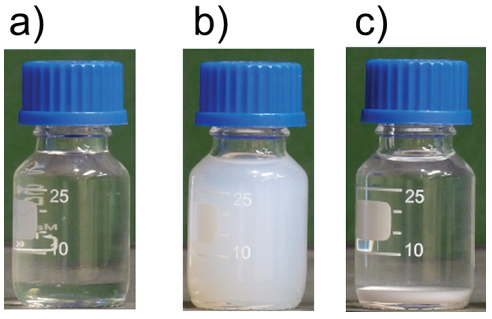

Figure 4. Evaluation of the colloidal stability of ZnO quantum dots. Images of ethanolic suspensions of ZnO nanoparticles synthesized with reactant ratio $[Zn^{2+}]/[OH^-]$ of (a)1/1, (b) 1/1.5, and (c) 1/2 stored for about 2 days at 20 °C.

unambiguously applicable as an *a priori* criterion for colloidal stability as the differences between the interaction potentials are very small and strongly dependent on particle size and several other parameters. Moreover, the two influencing factors on colloidal stability, the magnitude of the surface charge and the thickness of the protecting layer of molecules at the surface, superimpose each other within the calculations.

Stability of ZnO Quantum Dots. As it was already depicted, the progress of the ZnO crystal growth while the suspensions of the ZnO nanoparticles were aged in their mother liquors at 20 °C and 35 °C was monitored by recording UV–vis absorption spectra with time at a concentration of 0.05 mol L^{-1} (with respect to the Zn^{2+} concentration). Figure 3 shows exemplarily the absorption spectra of a ZnO suspension synthesized with the reactant ratio $[Zn^{2+}]/[OH^-]$ of 1/2 at 20 °C between 300 nm and 400 nm recorded immediately after precipitation (about 2 min) and afterward recorded automatically in appropriate time intervals for about 12 h as shown in Figure 3. Just after mixing the two reactants, the first absorption spectrum shows a well-defined extinction onset at about 325 nm. Thus, nucleation is supposed to be very fast at high supersaturations as it is not possible to resolve any induction period. In addition, a remarkable red shift in the absorption edge during the aging process is observed due to the quantum size effect indicating an increase of the particle size. These results imply that the particle size kept on evolving while their suspensions were stored at 20 °C and 35 °C. However, from the UV–vis absorption measurements not only information about the size of the nanoparticles is obtained. In the case of the ZnO quantum dots the absorption spectra measured below 5 h of aging additionally indicate also that the particles are stable in suspension without noticeable aggregation. With a mean diameter below 10 nm the particles are clearly situated in the Rayleigh regime. Thus, their scattering contribution toward the overall extinction measured is negligible. When the diameter of the particles increases due to growth and/or aggregation scattering occurs and the extinction at $\lambda > 400$ nm is nonzero.[32] In line with our previous observations[16,26] the ZnO particle growth for particles exceeding a size of 12 nm is extremely slow and can thus be neglected. Accordingly, the only process that takes place in the suspension is particle aggregation which is the origin for scattering as observed in the case of the suspension with the reactant ratios of 1/2 aged more than 5 h at 20 °C (Figure 3).

TABLE 2. Colloidal Stability of the ZnO Quantum Dots during 20 h of Aging at 20 °C

	stability		
	$[Zn^{2+}]/[OH^-] = 1/1$	$[Zn^{2+}]/[OH^-] = 1/1.5$	$[Zn^{2+}]/[OH^-] = 1/2$
unwashed	stable for >20 h	stable for less than 20 h	stable for less than 20 h
1× washed	stable for >20 h	stable for >20 h	stable for >20 h
2× washed	stable for >20 h	stable for less than 20 h	stable for less than 3 h
3× washed	stable for less than 3 h	stable for less than 3 h	stable for less than 3 h

Hence, the measurements of absorption spectra provide a convenient way to investigate colloidal stability of the ZnO quantum dots which is similar to the procedure described by Luo *et al.*[33] for zirconia (ZrO_2) nanocrystals.

Additionally, agglomeration was easily identified "by eye" as when aggregation commences a remarkable turbidity of the previously clear suspensions was observed as it is exemplarily shown in Figure 4. When a suspension turns turbid (Figure 4b) this indicates that a weak flocculation/aggregation of the ZnO nanoparticles occurs. Then, particle sedimentation (Figure 4c) is observed indicating that the ZnO nanoparticles are subject to significant aggregation.

Therefore, to define the colloidal stability of the ethanolic suspensions of all the different synthesis conditions, the following steps were performed: (i) At first, it was checked if the particles could be redispersed just by the addition of ethanol after precipitation with heptane. Regarding highly unstable suspensions such as the case for a reactant ratio of 1/2 after the second washing cycle, this was impossible for both temperatures. (ii) Then, the turbidity of the suspension was investigated by an extinction measurement at 400 nm. A clear, nonscattering suspension was considered as stable. Turbid suspensions with an extinction at a wavelength of $\lambda = 400$ nm which exceeded more than 1% of the extinction measured at the wavelength of the absorption maximum were considered as not stable. The results of the stability at 20 °C which were also used for the calculation of the dimensionless characteristic numbers shown in the following section are listed in Table 2.

The results for the suspensions synthesized and redispersed at 35 °C were derived accordingly and are shown in the Supporting Information (S4). However, the meaning of stability is somehow difficult to define. According to the literature, stability is the time until the first formation of doublets takes place which is in practice impossible to measure for nanoparticles with a diameter below 10 nm.[34] Therefore, we noted the scattering at fixed time intervals, namely after 3 h and 20 h after redispersion.

Dimensional Analysis. To identify the main influencing parameters, the well-established method of dimensional analysis was used, which is a simple but effective way of getting insight into the relevant physical relationships involved. Usually, this analysis is applied in the field of similarity theory and scale up, where it helps to identify decisive parameters and to reduce the number of independent variables necessary to describe a given problem by defining dimensionless numbers.[23] Regarding colloidal stability we have selected the following 14 variables: particle diameter x [m], shell thickness d [m], mean particle distance a [m], Debye-length κ^{-1} [m], which describes the thickness of the electric double layer in dependence of ionic strength, ζ-potential ζ [kg m^2 s^{-3} A^{-1}], permittivity ε' [A^2 s^4 kg^{-1} m^{-3}] which is the product of vacuum permittivity ε_0 [A^2 s^4 kg^{-1} m^{-3}] and relative permittivity ε_r [−], Hamaker constant A_{131} [kg m^2 s^{-2}], Boltzmann constant k_B [kg m^2 s^{-2} K^{-1}], temperature T [K], dynamic viscosity of the solvent η [kg m^{-1} s^{-1}], convective velocity v_{conv} [m s^{-1}], diffusion coefficient D [m^2 s^{-1}], fluid density ρ_F [kg m^{-3}], and doublet formation time t_D [s]. The particle density has been neglected since we do not consider external field forces which might become relevant in the case of nanoparticles in an ultracentrifuge, for instance, where a strong centrifugal field is present. According to the well-known Buckingham theorem these 14 variables can be reduced to 9 dimensionless numbers as we have to consider 5 basic units: length (L), time (T), mass (M), temperature (Θ) and current (I). The dimensionless numbers are defined as follows:

$$\Pi_1 = \frac{d}{x} = G$$

$$= \text{dimensionless steric contribution to stabilization } [-] \quad (2)$$

$$\Pi_2 = \frac{x}{a} = \frac{1}{\left(\frac{\pi}{6\,c_v}\right)^{1/3} - 1} = C$$

$$\text{scales with volume fraction } c_v\ [-] \quad (3)$$

$$\Pi_3 = \frac{A_{131}}{k_B T} = F_A = \frac{E_{vdW}}{E_{therm}}\ [-] \quad (4)$$

$$\Pi_4 = \frac{\varepsilon' x \zeta^2}{k_B T} = R = \frac{E_{DL}}{E_{therm}}\ [-] \quad (5)$$

$$\Pi_5 = a_\kappa = A_\kappa$$

$$= \text{dimensionless thickness of the electric double layer } [-] \quad (6)$$

$$\Pi_6 = \frac{\eta}{D\rho_F} = Sc\,[-] \quad (7)$$

$$\Pi_7 = \frac{v_{conv}x^2\,\eta}{k_BT}\,[-] \quad (8)$$

$$\Pi_8 = \frac{\rho_F\,k_BT}{x\,\eta^2}\,[-] \quad (9)$$

$$\Pi_9 = \frac{k_BTt_D}{x^3\eta} = \tau_P = \text{dimensionless process time}\,[-] \quad (10)$$

The set of Π-numbers defines Π_1 as a geometrical measure for the steric contribution, as it considers the effective thickness of the acetate layer *d* relative to the particle size *x* which will be named *G* in the following (eq 2). Second, Π_2 is the particle size *x* divided by the mean distance between the particles *a* and thus scales with the volume fraction c_v of the particles in the solvent. It will be named *C* in the following (eq 3). The mean distance was calculated according to Marczak *et al.* under the assumption of a regular cubic packing.[16] The attractive van der Waals interaction energy given by the Hamaker constants of the solid material and the solution[16] A_{131} is related to the thermal energy k_BT expressed by Π_3 (eq 4). Π_4 which we will further call *R* relates the energy of the double layer E_{DL} (including the ζ potential as a measure for the surface potential) toward thermal energy E_{therm} (eq 5).

Π_5 (eq 6) relates the mean distance between the particles *a* to the thickness of the double layer which is described by the Debye length κ^{-1}. Accordingly, for $\Pi_5 > 1$ the particles do not "see" each other, whereas for $\Pi_5 < 1$ neighboring particles always "feel" the presence of each other. As we already discussed in our previous work, the influence of the ionic strength which is needed for the calculation of κ^{-1} is not significant since all the experiments have been performed in organic solvent. In aqueous systems, however, this parameter may be more important.

Additionally, several well-known dimensionless parameters describing mass transport phenomena are found. Π_6 (eq 7) is the Schmidt number, *Sc*, taking into account the ratio of mass transfer by viscous (convective) transport and molecular diffusion. Multiplication of Π_6 (eq 7), Π_7 (eq 8), and Π_8 (eq 9) leads to the well-known Peclet number, *Pe*, which gives the ratio between convection and diffusion.[34] For our further considerations *Pe* is negligible because we only take into account quiescent liquids. Thus, *Pe* is zero for all the experiments investigated, as the particles were stored without stirring or shaking leading to $v_{conv} = 0$. The multiplication of Π_7 (eq 8) and Π_8 (eq 9) leads to the Reynolds number, *Re*, as the ratio of inertial and viscous forces which is again zero.

The last dimensionless number Π_9 (eq 10) includes the time t_D which is needed to form the first doublet out of two single particles and thus represents the dimensionless process time τ_P. This characteristic doublet formation time is linked with the stability ratio *W* under consideration of the volume fraction c_V by:[34]

$$t_D = \frac{\pi\eta x^3 W}{c_V k_B T} \quad (11)$$

Thus, the dimensionless process time to form the first doublet can be expressed as a set of dimensionless variables:

$$\tau_P = f\{\underbrace{R, F_A, G, A_{\kappa'}}_{\text{particle interactions}},\ C,\ \underbrace{Sc, Re, Pe}_{\text{mass transport}}\} \quad (12)$$

The influence of *Re* and *Pe* vanishes in quiescent liquids which we consider in this study. We already showed in the section about DLVO theory that the *W*-values for the quantum dots are generally small and not easy to interpret. Taking further into account that the doublet formation time for quantum dots is currently inaccessible by experiments, we will concentrate on *G*, *C*, F_A, *R*, and *Sc* to explain the stability. Relating the dimensionless repulsion *R* (eq 5) to the dimensionless attraction F_A (eq 4) and further relating the mass transport of the particles *Sc* (eq 7) to the dimensionless volume fraction *C* (eq 3) a stability parameter $(R/F_A)(Sc/C)$ is derived which we will call *S* in the following. This enables not only an analysis of data determined for the ZnO quantum dots which were described within the previous sections but also the extension to data obtained for various particle sizes, solid concentrations, temperatures, and material systems that are already introduced in the literature.

Stability Map. Figure 5 shows the results of *G* plotted against *S* for the different reactant ratios. Regarding the ZnO quantum dots the ζ-potential, the particle size *x*, and the weight loss of molecules attached to the particle surface at 20 and 35 °C, respectively, were measured by dynamic light scattering (DLS), UV−vis absorption spectroscopy, and TGA. From the surface coverage the shell thickness *d* was calculated using eq 1 and the diffusion coefficient *D* was calculated from the well-known Stokes−Einstein equation. The Hamaker constants of the solid materials A_{11} and the solvents A_{33}, respectively, as well as the permittivity ε′ for both temperatures were taken from literature data.[35,36]

Furthermore, *G* and *S* were calculated for ZnO quantum dots functionalized with larger molecules at the surface with possible application in dye-sensitized solar cells (DSSCs), that is, 4-*tert*-butyl-1-(3-(3,4-dihydroxybenzamido)benzyl)pyridinium bromide (CAMOBE), 1,1′-(5-(3,4-dihydroxybenzamido)-1,3-phenylene)bis(methylene)bis(4-*tert*-butylpyridinium) bromide

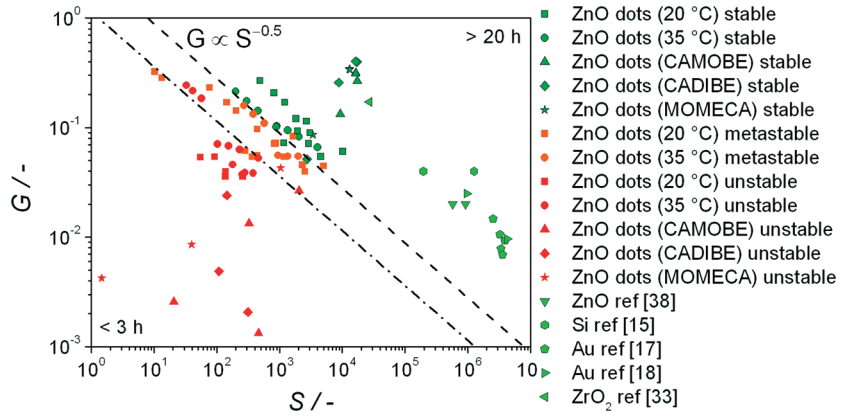

Figure 5. Geometry factor *G* against dimensionless interaction *S* (consisting of dimensionless repulsion *R*, dimensionless attraction F_A, dimensionless concentration *C* and the Schmidt number *Sc*, respectively) of ZnO quantum dots for the three different reactant ratios synthesized at 20 °C (squares) and 35 °C (circles). Additionally, the dimensionless numbers for quantum dots stabilized with CAMOBE (triangles up), CADIBE (diamonds), and MOMECA (stars), as well as larger ZnO nanoparticles (triangles down) and other material systems like Si (hexagons), Au (pentagons and triangles right), and ZrO_2 (triangles left) are shown. Red color indicates unstable suspensions, orange color represents metastable regions, and dark as well as light green color indicates suspensions which are stable for more than 20 h.

Chart 1. Cationic dendrons: (a) CAMOBE, (b) CADIBE, and (c) MOMECA

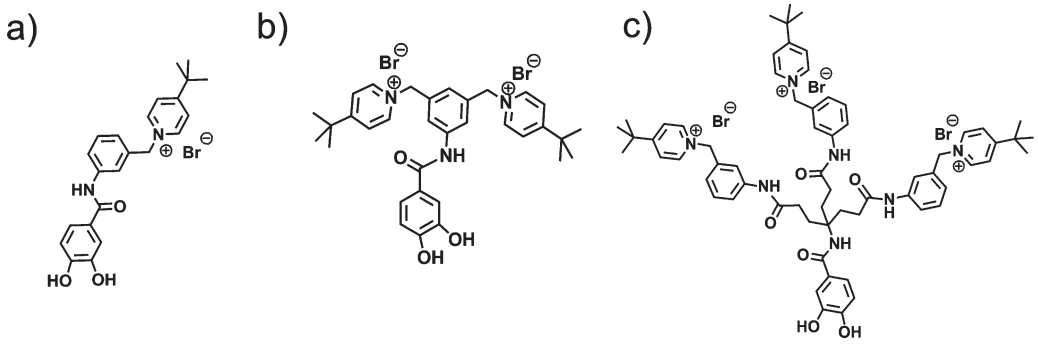

(CADIBE) and *N*1,*N*7-bis(3-(4-*tert*-butyl-pyridium-methyl)-phenyl)-4-(3-(3-(4-*tert*-butyl-pyridinium-methyl)phenyl-amino)-3-oxopropyl)-4-(3,4-dihydroxybenzamido)hepta-nediamide tribromide (MOMECA), shown in Chart 1.[37] Finally, the stability map is extended to literature data given for larger ZnO nanoparticles in ethanol and water,[38] silicon in water and butanol,[15] citrate stabilized gold nanoparticles in aqueous solution,[17,18] as well as ZrO_2 in water[33] as a ceramic oxide material. However, literature values including all data necessary for the evaluation of unstable working points were not found. Usually, only data about stable systems is provided. A detailed list of the values used for the calculation of each number is found in the Supporting Information (S5).

The *G*—*S* plot shows a stable (Figure 5, dark and light green data points) region without any agglomeration for more than 20 h independent from the molecules present at the surface, the solid concentration, the diffusivity, and the material system. The temperature influence is mainly reflected by *Sc* as it includes the diffusion coefficient and the viscosity of the solvent which are both strongly temperature dependent. Furthermore, a metastable region (Figure 5, orange data points) without agglomeration for more than 3 h but less than 20 h as well as an unstable region (Figure 5, red data points) with agglomeration during the first 3 h after redispersion is identified. As expected, with increasing surface charge of the nanoparticles or increasing shell thickness the data points are shifted into the stable region. The transition between the different areas (stable, metastable, unstable) is shown with orange data points.

From Figure 5 it becomes clear that the transition between the different regions is described by a power law as *G* scales with $S^{-0.5}$. However, the exact position of the transient regime between stable and unstable suspensions depends on the chosen definition of colloidal stability and might slightly change if more experimental values, for example, for other material systems, are added. The observed correlation finally leads to the following expression for suspensions entering the next stable region with a constant factor

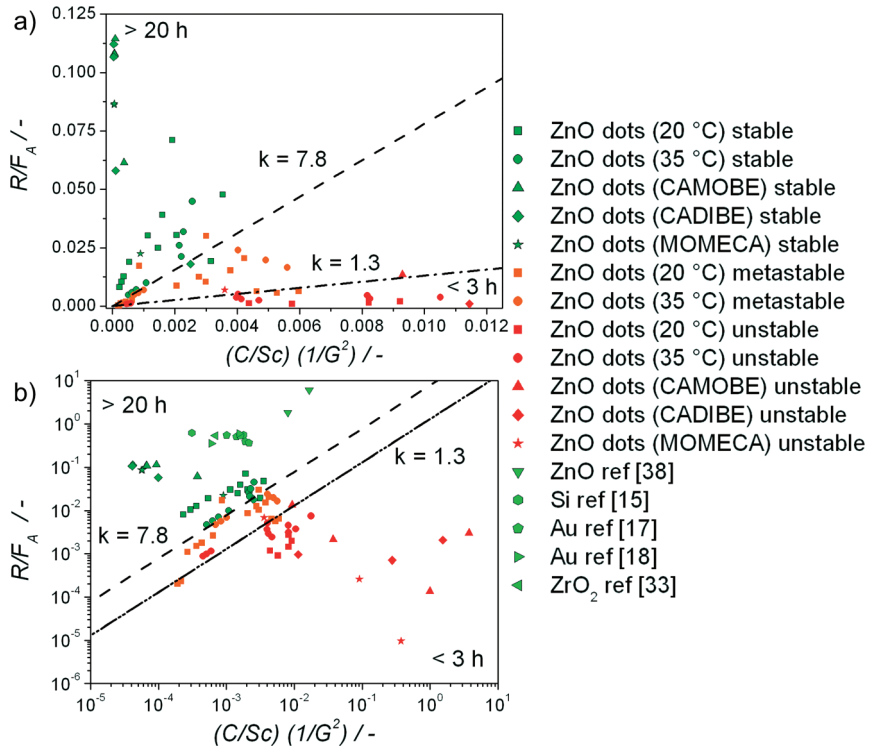

Figure 6. Graphic evaluation of eq 13 with linear axis scale (a) and logarithmic axis scale (b); the symbols are arranged according to Figure 5.

k which depends on the time t_S until the first scattering due to agglomeration is observed:

$$\frac{\pi_4}{\pi_3} = \frac{R}{F_A} = \frac{\varepsilon' x \zeta^2}{A_{131}} > k(t_S) C Sc^{-1} G^{-2}$$

$$= k(t_S)\left(\frac{x}{a}\right)\left(\frac{\eta_F}{\rho_F D}\right)^{-1}\left(\frac{d}{x}\right)^{-2} \quad (13)$$

Thereby $k(t_s = 3\ \text{h}) = 1.3$ and $k(t_s = 20\ \text{h}) = 7.8$. The graphic solution for these findings is shown in Figure 6. In addition to the logarithmic scale Figure 6a shows a linear plot to evidence that the regions are, except four outliers, clearly within the borderlines described by eq 13.

Consequently, the relation between repulsion and attraction is solely determined by volume fraction, mass transfer in a way that conditions for stable suspensions are easily identified. Currently, the exact functional relationship between the original target quantity τ_P and the influencing factors is still unknown as the time resolution would have to be much finer to derive a kinetic expression. However, we assume the following relation (while still neglecting external forces):

$$\tau_P(k(t)) = f\left(\underbrace{\frac{R}{F_A}\cdot G^2}_{\text{interactions}} \cdot \underbrace{Sc}_{\text{transport}} \cdot \underbrace{C^{-1}}_{\text{concentration}}\right) \quad (14)$$

From coagulation theory of monodisperse particles we know that the following kinetic equation holds:

$$-\frac{dN}{dt} = \underbrace{\frac{1}{W}}_{\substack{\text{particle}\\ \text{interactions}}} \cdot \underbrace{\beta}_{\text{transport}} \cdot \underbrace{N^2}_{\text{concentration}} \quad (15)$$

The solution of this equation with respect to time leads to $t = f(W, \beta, N)$, that is, $\tau_P = f$(interactions, transport, concentration). The dimensionless numbers proposed include obviously all relevant parameters that are considered in the usual approach. The time until agglomeration commences depends (i) on the collision kernel which is related to the mass transport of the particles within a suspension, (ii) on the particle−particle interactions which decide if two particles stick together or not, and (iii) on the particle concentration.

Our stability map covers so far the following range of parameters: the Hamaker constants of the material A_{11} and the solvent A_{33}, the particle diameter x and the shell thickness d, the ζ-potential, the dielectric properties of the solvent ε', the mean distance a between the nanoparticles as a measure for the solid concentration, the viscosity of the solvent η, the density of the solvent ρ_F, and the diffusion coefficient D. Thereby, the data range covers 7 orders of magnitude regarding the stability parameter S and 3 orders of magnitude regarding the geometry factor G. For the particle sizes the maximum particle size of 100 nm in the case of the Si-nanoparticles was considered, whereas the smallest particle size of about 2 nm was considered for

ZnO.[15,38] For larger particles, solvents of higher viscosities or stirred suspensions we expect that a function depending on the Reynolds number would be needed. Also the Peclet number will have to be included when assumptions such as purely diffusion driven phenomena ($Pe = 0$) are not valid anymore.

Regarding the other limiting cases of our approach, namely a vanishing van der Waals attraction in refractive index matched situations, a vanishing ζ-potential in the case of pure steric stabilization, and finally systems without a stabilizing shell at all like pure oxide materials, the dimensionless numbers are expected to be still applicable: Vanishing van der Waals forces, meaning maximum stability, are leading to $S \rightarrow \infty$. Thus, independent of the geometry number the suspension is considered to be stable. A more difficult situation is expected for completely vanishing ζ-potential ($\zeta \rightarrow 0$). Then, d has to be sufficiently large to provide a good screening of the van der Waals attraction to prevent the particles to come too close into contact. In this case the properties of the shell at the solvent temperature have to be considered. In addition, the Hamaker constant of the shell should be close to that of the solvent, and any chemical interactions between the shells of different particles shall be negligible. These findings are in agreement with the unusual high stability of silica particles close to the isoelectric point reported in the literature, where water molecules or silicic acid are supposed to stabilize the particles.[39] Our model, however, does not consider attractive interactions between long chain molecules or any polymers with the solvent which are important in case of typical steric stabilization. Regarding systems without a surrounding stabilizing shell ($d \rightarrow 0$) a sufficiently high charge has to be present at the particle surface to reach a stable region.

CONCLUSION

In the present work the colloidal stability of ZnO quantum dots synthesized at 20 °C and 35 °C in ethanol with respect to the washing procedure was investigated. Thereby, the particle sizes were calculated from the absorption spectra, ζ-potentials and pH* were determined for different reactant ratios $[Zn^{2+}]/[OH^-]$, and an effective shell thickness with respect to a monolayer of acetate molecules around the particles was calculated from the weight losses during TGA. It could be concluded that the surface charge of the nanoparticles directly after synthesis is dominated by specific ion adsorption at the particle surface. Then, with ongoing washing a noticeable decrease of the ζ-potential is observed as the charge determining coordinating acetate ions are continuously removed. For an explanation of the colloidal stability calculations according to the DLVO theory were performed using a core–shell model and the stability ratio W was derived. The values of W for nanoparticles below 20 nm are small and difficult to interpret. To understand the experimental results not only the height of the maximum calculated with DLVO theory but also the depth of the primary minimum has to be considered. However, an unambiguous understanding of colloidal stability without experiments is impossible.

In the second part of the manuscript a dimensional analysis was performed. For 14 variables and 5 basic units, 9 independent Π-products were derived which comprise a geometric factor G and a stability parameter S. The latter includes the ratio between dimensionless repulsion R and dimensionless attraction F_A as well as the Schmidt number Sc and the dimensionless particle concentration C. Then, G and S were investigated in detail as they include the most important influencing factors found in the experiments. Those are the shell thickness, the ζ-potential, the overall permittivity, the Hamaker constants of the material and the solvent, the mean distance between the particles, the diffusivity and the viscosity as well as the density of the solvent. Regarding the ZnO quantum dots, a measurable criterion for colloidal stability was found which is based on UV–vis absorption measurements. Then, by plotting the geometry factor G against S and considering the time until detectable agglomeration commences, a stability map was established with an unstable, a metastable, and a stable region. The different regions are separated by a reciprocal power law ($G \propto S^{-0.5}$) meaning that the van der Waals attraction is compensated linearly by the electrostatic repulsion and the square of the acetate shell scaling with the surface. The present approach has the potential to establish a dimensionless agglomeration rate based on particle–particle interactions, collisions, and particle concentration. However, the borderline between the different regions is transient and the addition of new data points for other material systems is highly welcome. To evidence that our approach is extendible toward other solvents and stabilizing molecules as well as applicable toward other material systems, data for ZnO quantum dots for DSSCs as well as data from the literature for larger ZnO, Si, ZrO_2, and Au nanoparticles were included into the stability map. In contrast to DLVO calculations that lead to comparatively small values in the case of particles in the lower nanometer range, our approach helps to find optimal conditions for the stabilization of colloids in between the boundary conditions of refractive index matched situations ($F_A \rightarrow 0$), vanishing ζ-potentials ($R \rightarrow 0$), and pure surfaces without stabilizing molecules ($G \rightarrow 0$).

The understanding of colloidal stability and the separation of the different influencing factors is believed to be indispensable and one of the key steps for the successful incorporation of comparatively new materials into various future applications. Our approach might be transferred to other

quantum dots or nanoparticle dispersions to explain the unusual stability of nanoparticles in solvothermal synthesis where solvent molecules coordinate to the particle surface. This is seen to be decisive for a successful scale-up of nanoparticle synthesis from the lab-scale toward industrial applications.

MATERIALS AND METHODS

Synthesis and Purification of ZnO Quantum Dots Stabilized with Acetate. All chemicals were analytical grade reagents used without further purification. ZnO nanoparticles were obtained using a preparation procedure adapted from Spanhel *et al.*[40] and Meulenkamp.[41] The synthesis of the nanoparticles was performed as already described in the literature.[16] Thereby three different ratios of $ZnAc_2$/LiOH ($[Zn^{2+}]/[OH^-]$) were adjusted (with respect to the Zn^{2+} concentration): 1/1 (using a hydroxide concentration of 0.1 mol L^{-1}), 1/1.5 (using a hydroxide concentration of 0.15 mol L^{-1}) and 1/2 (using a hydroxide concentration of 0.2 mol L^{-1}). The particles were aged in their mother liquors at the synthesis temperature to achieve different particle sizes, before the purification was started by adding an excess of *n*-heptane. The details of the purification procedure are found elsewhere.[16]

Characterization of ZnO Quantum Dots and Sample Preparation. Optical properties of the ZnO nanoparticles were determined from UV–vis absorption spectra recorded using a Cary 100 Scan UV–visible spectrophotometer (Varian Deutschland GmbH, Germany) with cuvettes of 10 mm or 0.2 mm optical path length. The ζ-potentials of 0.05 mol L^{-1} ZnO ethanolic suspensions (with respect to the Zn^{2+} concentration) were obtained *via* DLS by using a Malvern Nano ZS Instrument (Malvern Instruments GmbH, Germany) by means of laser Doppler electrophoresis. The same concentration was used for determination of pH* measured with a solvotrode (Metrohm GmbH & Co. KG, Germany). TGA measurements were carried out on a Q50 Thermoanalyser (TA Instruments, USA). During the measurements a small amount of the investigated powder (about 15–20 mg) was heated from room temperature to 600 °C at a constant heating rate of 10 °C min^{-1} under a nitrogen flow of 60 mL min^{-1}. For the optical characterization by using UV–vis absorption spectroscopy and dynamic light scattering (DLS) as well as determination of pH*, the ZnO flocculates were easily redispersed in ethanol using sonication. For the compositional characterization by using TGA, the ZnO flocculates were dried under nitrogen for about 5 min at room temperature to obtain a solid powder. Furthermore, it has to be mentioned that the asterisk (*) after pH refers to a measurement in ethanolic solution. Thus, it is not the dissociation of water that is measured but the dissociation of ethanol.

ZnO Quantum Dots Stabilization with Cationic Dendrons. *Synthesis of the Cationic Dendrons.* To stabilize ZnO nanoparticles with cationic dendrons, that is, 4-*tert*-butyl-1-(3-(3,4-dihydroxybenzamido)benzyl)pyridinium bromide (CAMOBE), 1,1′-(5-(3,4-dihydroxybenzamido)-1, 3-phenylene)bis(methylene)bis(4-*tert*-butylpyridinium) bromide (CADIBE), and *N*1,*N*7-bis(3-(4-*tert*-butyl-pyridium-methyl)phenyl)-4-(3-(3-(4-*tert*-butyl-pyridinium-methyl)phenyl-amino)-3-oxopropyl)-4-(3,4-dihydroxybenzamido)-heptanediamide tribromide (MOMECA) (Chart 1), a completely new synthetic route has been developed and a detailed description of the whole synthesis procedure has been recently published.[37] A challenging step in the synthetic process chain is the generation of the cationic charge as well as the introduction of an anchoring group which is capable of anchoring on ZnO. We have reported on the strong binding between metalloporphyrins equipped with catechol anchoring groups and ZnO nanoparticles to construct DSSCs.[26] To establish a strong bonding, the use of a catechol anchoring group was reasonable. The key to our approach was a novel synthetic route generating highly reactive benzylic bromides which react readily with nucleophiles like pyridine resulting in quarternized N-atoms and generating permanent cationic charges in very high yields and outstanding purity. 3-Methoxymethylaniline and 3,5-bis-(methoxymethyl)aniline were successfully connected to carboxylic acid containing diphenylmethane-protected catechols. The benzylic methyl ethers were transformed quantitatively into the corresponding benzylic bromides and delivered in the same step as the deprotected catechol by means of hydrobromic acid. The cationic charges were obtained by the reaction of the benzylic bromides with 4-*tert*-butylpyridine leading to the quantitative formation of cationic charges.

ZnO Quantum Dots Surface Functionalization with the Cationic Dendrons.[26]. ZnO nanoparticles with a mean size of about 4.5 nm were synthesized with the reactant ratio $[Zn^{2+}]/[OH^-]$ = 1/1.5. The particles were aged in the mother liquor for 4 h at 30 °C and then washed three times as described above. Further, white ZnO flocculates obtained after the washing were redispersed in ethanol (concentrations of 0.05 mol L^{-1}) and mixed with different amount of the polycationic molecules in ethanol (concentrations from 5×10^{-6} to about 1×10^{-3} mol L^{-1}). The mixture was sonicated for 15 min for the sake of adsorption.

Acknowledgment. The authors would like to thank the German Research Council (DFG) for their financial support (Projects PE427/18-2 and Leibniz program) which supports within the framework of its Excellence Initiative the Cluster of Excellence "Engineering of Advanced Materials" (www.eam.uni-erlangen.de) at the University of Erlangen-Nuremberg. Furthermore, we thank Stefan Romeis, Cornelia Damm, Claudia Eisermann, and Volodymyr Lobaz for helpful discussion.

Supporting Information Available: Growth data of ZnO nanoparticles, surface charge and ζ-potential of the nanoparticles, primary minima and stability ratios, data of colloidal stability and data used for the stability maps. This material is available free of charge *via* the Internet at http://pubs.acs.org.

REFERENCES AND NOTES

1. Segets, D.; Gradl, J.; Klupp Taylor, R.; Vassilev, V.; Peukert, W. Analysis of Optical Absorbance Spectra for the Determination of ZnO Nanoparticle Size Distribution, Solubility, and Surface Energy. *ACS Nano* **2009**, *3*, 1703–1710.
2. Segets, D.; Martinez Tomalino, L.; Gradl, J.; Peukert, W. Real-Time Monitoring of the Nucleation and Growth of ZnO Nanoparticles Using an Optical Hyper-Rayleigh Scattering Method. *J. Phys. Chem. C* **2009**, *113*, 11995.
3. Viswanatha, R.; Amenitsch, H.; Sarma, D. D. Growth Kinetics of ZnO Nanocrystals: A Few Surprises. *J. Am. Chem. Soc.* **2007**, *129*, 4470–4475.
4. Viswanatha, R.; Santra, P. K.; Dasgupta, C.; Sarma, D. D. Growth Mechanism of Nanocrystals in Solution: ZnO, a Case Study. *Phys. Rev. Lett.* **2007**, *98*, 255501/1–255501/4.
5. Faber, H.; Burkhardt, M.; Jedaa, A.; Kälblein, D.; Klauk, H.; Halik, M. Low-Temperature Solution-Processed Memory Transistors Based on Zinc Oxide Nanoparticles. *Adv. Mater.* **2009**, *21*, 1–6.
6. Hagfeldt, A.; Grätzel, M. Molecular Photovoltaics. *Acc. Chem. Res.* **2000**, *33*, 269.
7. Quintana, M.; Edvinsson, T.; Hagfeldt, A.; Boschloo, G. Comparison of Dye-Sensitized ZnO and TiO_2 Solar Cells: Studies of Charge Transport and Carrier Lifetime. *J. Phys. Chem. C* **2007**, *111*, 1035–1041.
8. Werner, F.; Gnichwitz, J.-F.; Marczak, R.; Palomares, E.; Peukert, W.; Hirsch, A.; Guldi, D. M. Grafting Porphyrins (Face-to-Edge/Orthogonal *versus* Face-to-Face/Parallel) to ZnO en Route toward Dye-Sensitized Solar Cells. *J. Phys. Chem. B* **2010**, *114*, 14671–14678.
9. Sperling, R. A.; Parak, W. J. Surface Modification, Functionalization and Bioconjugation of Colloidal Inorganic Nanoparticles. *Phil. Trans. R. Soc. A* **2010**, *368*, 1333–1383.

10. Garnweitner, G.; Ghareeb, H. O.; Grote, C. Small-Molecule *in Situ* Stabilization of TiO_2 Nanoparticles for the Facile Preparation of Stable Colloidal Dispersions. *Coll. Surf. A: Physicochem. Eng. Aspects* **2010**, *372*, 41–47.
11. Pachón, L. D.; Rothenberg, G. Transition-Metal Nanoparticles: Synthesis, Stability and the Leaching Issue. *Appl. Organometal. Chem.* **2008**, *22*, 288–299.
12. Derjaguin, B. V.; Landau, L. D. A Theory of the Stability of Strongly Charged Lyophobic Sols and the Coalescence of Strongly Charged Particles in Electrolytic Solution. *Acta Phys. URSS* **1941**, *14*, 633.
13. Verwey, E. J. W.; Overbeek, T. G. *Theory of the Stability of Lyophobic Colloids*; Elsevier: Amsterdam, The Netherlands, 1948.
14. Lagaly, G.; Schulz, O.; Zimehl, R. *Dispersionen und Emulsionen;* Steinkopff: Darmstadt, Germany, 1997.
15. Reindl, A.; Peukert, W. Intrinsically Stable Dispersions of Silicon Nanoparticles. *J. Colloid Interface Sci.* **2008**, *325*, 173–178.
16. Marczak, R.; Segets, D.; Voigt, M.; Peukert, W. Optimum between Purification and Colloidal Stability of ZnO Nanoparticles. *Adv. Powder Technol.* **2010**, *21*, 41–49.
17. Kim, T.; Lee, K.; Gong, M.; Joo, S.-W. Control of Gold Nanoparticle Aggregates by Manipulation of Interparticle Interaction. *Langmuir* **2005**, *21*, 9524–9528.
18. Kim, T.; Lee, C.-H.; Joo, S.-W. Kinetics of Gold Nanoparticle Aggregation: Experiments and Modeling. *J. Colloid Interface Sci.* **2008**, *318*, 238–243.
19. Noh, M.; Kim, T.; Lee, H.; Kim, C.-K.; Joo, S.-W.; Lee, K. Fluorescence Quenching Caused by Aggregation of Water-Soluble CdSe Quantum Dots. *Coll. Surf. A* **2010**, *359*, 39–44.
20. Kim, B.-S.; Lobaskin, V.; Tsekov, R.; Vinogradova, O. I. Dynamics and Stability of Dispersions of Polyelectrolyte-Filled Multilayer Microcapsules. *J. Chem. Phys.* **2007**, *126*, 244901.
21. Sabin, J.; Prieto, G.; Sennato, S.; Ruso, J. M.; Angelini, R.; Bordi, F.; Sarmiento, F. Effect of Gd^{3+} on the Colloidal Stability of Liposomes. *Phys. Rev. E* **2006**, *74*, 031913.
22. Yadav, P. S.; Dupre, D.; Tadmor, R.; Park, J. S.; Katoshevski, D. Effective Refractive Index and Intermolecular Forces Associated with a Phase of Functional Groups. *Surf. Sci.* **2007**, *601*, 4582.
23. Zlokarnik, M. *Dimensional Analysis and Scale-up in Chemical Engineering*; Springer Verlag: Berlin- Heidelberg, 1991.
24. Sakohara, S.; Ishida, M.; Anderson, M. A. Visible Luminescence and Surface Properties of Nanosized ZnO Colloids Prepared by Hydrolyzing Zinc Acetate. *J. Phys. Chem. B* **1998**, *102*), 10169–10175.
25. Marczak, R.; Werner, F.; Ahmad, R.; Lobaz, V.; Guldi, D. M.; Peukert, W. Detailed Investigations of ZnO Photoelectrodes Preparation for Dye Sensitized Solar Cells. *Langmuir* **2011**, *27*), 3920–3929.
26. Marczak, R.; Werner, F.; Gnichwitz, J.-F.; Hirsch, A.; Guldi, D. M.; Peukert, W. Communication *via* Electron and Energy Transfer between Zinc Oxide Nanoparticles and Organic Adsorbates. *J. Phys. Chem. C* **2009**, *113*, 4669–4678.
27. Tang, X.; Choo, E. S. G.; Li, L.; Ding, J.; Xue, J. Synthesis of ZnO Nanoparticles with Tunable Emission Colors and Their Cell Labeling Applications. *Chem. Mater.* **2010**, *22*, 3383–3388.
28. Spanhel, L.; Anderson, M. A. Semiconductor Clusters in the Sol–Gel Process: Quantized Aggregation, Gelation, and Crystal Growth in Concentrated Zinc Oxide Colloids. *J. Am. Chem. Soc.* **1991**, *113*, 2826–2833.
29. Schwarz, U. S.; Safran, S. A. Phase Behavior and Material Properties of Hollow Nanoparticles. *Phys. Rev. E* **2000**, *62*, 6957–6967.
30. Tadmor, R.; Klein, J. H. Additional Attraction between Surfactant-Coated Surfaces. *J. Colloid Interface Sci.* **2002**, *247*, 321–326.
31. Israelachvili, J. *Intermolecular and Surface Forces*; Academic Press: London, 1991.
32. Viswanatha, R.; Sapra, S.; Satpati, B.; Satyam, P. V.; Dev, B. N.; Sarma, D. D. Understanding the Quantum Size Effects in ZnO Nanocrystals. *J. Mater. Chem.* **2004**, *14*, 661–668.
33. Luo, K.; Zhou, S.; Wu, L.; Gu, G. Dispersion and Functionalization of Nonaqueous Synthesized Zirconia Nanocrystals *via* Attachment of Silane Coupling Agents. *Langmuir* **2008**, *24*), 11497–11505.
34. Russel, W. B.; Saville, D. A.; Schowalter, W. R. *Colloidal Dispersions*; Cambridge University Press: 1989.
35. Azouni, M. A.; Casses, P.; Sergiani, B. Capture or Repulsion of Treated Nylon Particles by an Ice–Water Interface. *Coll. Surf. A* **1997**, *122*, 199–205.
36. Schmid, H. Kinetische Ermittlung Der Enthalpie Und Entropie Innerer Wasserstoffbrückenbindungen von Anionen. *Monatsh. Chem.* **1969**, *100*, 1654–1661.
37. Gnichwitz, J. F.; Marczak, R.; Werner, F.; Lang, N.; Jux, N.; Guldi, D. M.; Peukert, W.; Hirsch, A. Efficient Synthetic Access to Cationic Dendrons and Their Application for ZnO Nanoparticles. *J. Am. Chem. Soc.* **2010**, *132*, 17910–17920.
38. Reindl, A. Dispersing and Stabilizing Semiconducting Nanoparticles for Application in Printable Electronics. Doctoral Thesis, University Erlangen-Nuremberg, Erlangen, 2009.
39. Colic, M.; Fisher, M. L.; Franks, G. V. Influence of Size on Short-Range Repulsive Forces between Silica Surfaces. *Langmuir* **1998**, *14*, 6107–6112.
40. Spanhel, L.; Weller, H.; Henglein, A. Photochemistry of Semiconductor Colloids. 22. Electron Injection from Illuminated CdS into Attached TiO_2 and ZnO Particles. *J. Am. Chem. Soc.* **1987**, *109*, 6632.
41. Meulenkamp, E. A. Synthesis and Growth of ZnO Nanoparticles. *J. Phys. Chem. B* **1998**, *102*, 5566–5572.